Title

Precise isolation and structural origin of an ultra-specific nanobody against chemical compound

Authors

Yang, Huijuan
Vasylieva, Natalia
Wang, Jiaxin
et al.

Publication Date

2023-09-01

DOI

10.1016/j.jhazmat.2023.131958

Peer reviewed

HHS Public Access

Author manuscript

J Hazard Mater. Author manuscript; available in PMC 2024 September 15.

Published in final edited form as:

J Hazard Mater. 2023 September 15; 458: 131958. doi:10.1016/j.jhazmat.2023.131958.

Precise isolation and structural origin of an ultra-specific nanobody against chemical compound

Huijuan Yang[a], **Natalia Vasylieva**[b], **Jiaxin Wang**[a], **Zhenfeng Li**[b], **Wenbo Duan**[a], **Shuang Chen**[a], **Kai Wen**[a], **Hui Meng**[c], **Xuezhi Yu**[a], **Jianzhong Shen**[a], **Bruce D. Hammock**[b], **Zhanhui Wang**[*,a]

[a]National Key Laboratory of Veterinary Public Health Security, College of Veterinary Medicine China Agricultural University, Beijing Key Laboratory of Detection Technology for Animal-Derived Food Safety, and Beijing Laboratory for Food Quality and Safety, Beijing 100193, China

[b]Department of Entomology and UCD Comprehensive Cancer Center, University of California, Davis, CA 95616, United States

[c]School of the Environment and Safety Engineering, Jiangsu University, Zhenjiang 212013, Jiangsu, China

Abstract

Highly specific antibodies are the key reagents for developing immunoassays with a low false positive rate for environmental monitoring. Here, we provide evidence that nanobodies have the potential to achieve higher specificity than conventional antibodies and explain why from their structural features. Using sulfadimethoxine (SDM) as a model analyte, we constructed an immune phage display library and precisely isolated an ultra-specific nanobody (H1–17) by a crucial homologous antigen counter selection strategy. H1–17 showed no observable cross-reactivity (CR) with other structural analogs of 41 SDM tested, which has never been achieved by conventional antibodies. The structurally original specificity of H1–17 was illuminated and compared with that of one conventional antibody by homology modeling and site-directed mutagenesis validation. It was found that the noncanonical disulfide bond (C50-C104) of H1–17 helped CDR3 form a tailor-made binding pocket and divide it into two parts to accommodate the common structure of sulfonamides and the characteristic methoxyl group of SDM, respectively. Besides, the mutual-checking hydrogen bonds also played important roles in the specific recognition. Lastly, immunoassays with zero false positive rate were developed to screen SDM in water and milk

[*]Author to whom correspondence should be addressed: Tel: +86-10-6273 4565, Fax: +86-10-6273 1032, wangzhanhui@cau.edu.cn.

CRediT authorship contribution statement

Huijuan Yang: Conceptualization, Investigation, Formal analysis, Writing-original draft, Funding acquisition. Natalia Vasylieva: Formal analysis, Visualization, Writing-review & editing. Jiaxin Wang: Methodology, Visualization. Zhenfeng Li: Investigation, Formal analysis, Writing-review & editing. Wenbo Duan: Methodology, Visualization. Shuang Chen: Methodology, Visualization. Kai Wen: Validation, Visualization. Hui Meng: Investigation, Methodology. Xuezhi Yu: Data curation, Funding acquisition. Jianzhong Shen: Conceptualization, Resources, Supervision. Bruce D. Hammock: Resources, Writing-review & editing, Funding acquisition. Zhanhui Wang: Conceptualization, Writing-review & editing, Funding acquisition, Project administration.

Declaration of Competing Interest

The authors declare that they have no known competing financial interests or personal relationships that could have appeared to influence the work reported in this paper.

Appendix A. Supplementary material

Supplementary data to this article is available.

samples, indicating that nanobodies could be reliable reagents for the accurate detection of chemical compounds.

Keywords

Nanobody; Ultra-specificity; Recognition mechanism; Immunoassay; Accurate detection

1. Introduction

Immunoassays for chemical compounds have been widely used in many fields such as environmental pollutants monitoring, food safety analysis, and clinical diagnostics due to their inherent specificity, high sensitivity, easy operation, and short assay time (Wild, 2013). As the critical recognition elements in immunoassays, antibodies were identified with sufficient specificity to discriminate marginally different analytes from structurally similar analogs, even as less as a single functional group or even chirality (Landsteiner, 2013). However, the lack of specificity of antibodies with some analytes has always practically presented difficulties (Prassas and Diamandis, 2014). There is accumulating evidence that many antibodies can inevitably bind to different structurally-related compounds with varied affinities, a phenomenon generally referred to as cross-reactivity (CR) (Jain and Salunke, 2019; Michel et al., 2009). Unexpected CRs will cause serious false positive results and an inexact quantification of the analyte of interest (Egelhofer et al., 2011; Baker, 2015; Peveler et al., 2016).

CR occurs because the antibody is a mixture of immune globulins with multiple specificities, or simply because the antibody could bind to more than one analyte sharing a similar epitope. To avoid the former problem, a monoclonal antibody (mAb) should be produced as a real mAb, which should include the prevention of contaminations by other antibodies during the production phase in the abdominal cavity of animals (Bordeaux et al., 2010) and the avoiding of the expression of additional functional variable regions in hybridomas (Bradbury et al., 2018). Regarding the latter problem, employing an intentional counter selection step, such as a carefully designed panning strategy to characterize and limit CR during antibody isolation, will be a prudent solution. It seems that the emerging nanobodies, the variable domain of naturally occurring camelid heavy-chain-only antibodies (VHHs), are more promising reagents produced by using an intentional counter selection step strategy (Hamers-Casterman et al., 1993; Ingram et al., 2018). Because nanobodies can be easily produced as single clones based on their unique sequences and the phage display technology used to obtain nanobodies has higher efficiency and flexibility during the isolation process (Bradbury and Plückthun, 2015; Peltomaa et al., 2019). Besides, compared with other antibodies, nanobodies have the smallest size (1/10th the size of conventional antibodies), and the highest stability, and they have novel structural conformations of paratopes that can bind to antigens in ways that cannot be accomplished by other antibodies (Muyldermans et al., 2009; Stijlemans et al., 2004; Genst et al., 2006; Zhang et al., 2019; He et al., 2020). Since chemical compounds belong to haptens and can only provide limited epitopes, nanobodies can be potentially more specific than conventional antibodies derived

from mice or rabbits with proper selection and genetic manipulation (Deckers et al., 2009; Li et al., 2018).

Sulfadimethoxine (SDM) is a long-acting broad-spectrum antimicrobial agent of sulfonamide (SA) with a common structure of para-aminobenzenesulfonamide, which is widely used in livestock and aquacultures. Due to its large usage and hard-biodegradable, SDM has been reported to be detected in various environmental media and animal-derived food (Zhuang et al., 2019; Ben et al., 2020). Residual SDM can cause bacterial resistance, affect ecological balance, and endanger human health through food chain enrichment (Huang et al., 2020; Li et al., 2022). With the increasing problem of SDM residues, many countries have separately stipulated the maximum residue limit (MRL) of SDM in the latest regulations, rather than the MRL of total SAs. For example, Japan and the United States have set the MRLs for SDM of 20 μg/kg and 10 μg/kg in milk, respectively (The Japan Food Chemical Research Foundation, 2021; U.S. Food & Drug Administration, 2019). To meet these regulations, immunoassays with high specificity to discriminate between SDM and other structural analogs (Fig. 1A and Fig. 1B), thus avoiding the false positive risk, are highly needed. However, reported immunoassays for SDM detection always suffered varied CRs from other SAs mainly because the specificity of the employed antibody, even mAbs, showed more or less recognition ability to related SAs (Muldoon et al., 2000). Therefore, it is essential to prepare ultra-specific antibodies without any recognition of other SAs for accurate detection of SDM.

In this work, SDM was used as a model analyte to explore the potential of nanobodies in specificity for chemical compounds. Mouse mAb and the single-chain variable fragment (scFv) were also prepared to make the comparison. To precisely isolate the desired nanobodies from the phage display library, we proposed a homologous antigen counter selection strategy, which was proved to be efficient by comparing it with the heterologous antigen strategy and the standard hybridoma screening method. After fully characterizing the obtained nanobody, the recognition mechanism of the nanobody was further studied and compared with that of the mouse mAb to SDM and other anti-hapten nanobodies. The relationship between the ultra-specificity and the inherent structural characteristics of nanobody H1–17 was illuminated and one novel binding mode between nanobodies and chemical compounds was found. Finally, the performance of the nanobody in practical applications was evaluated by developing an immunoassay for the detection of SDM in water and milk samples.

2. Experimental section

2.1. Reagents and materials

Standards sulfadimethoxine (SDM), sulfadoxine (SDM'), sulfamonomethoxine (SMM), sulfameter (SMD), sulfalene (SLE), sulfamethoxypyridazine (SMP), sulfaethoxypyridazine (SEP), sulfisomidine (SIM), sulfamethazine (SMZ), sulfamerazine (SMR), sulfadiazine (SDZ), sulfabromomethazine (SBM), sulfachlorpyrazine (SCY), sulfachloropyridazine (SCP), sulfaquinoxaline (SQX), sulfapyridine (SPY), sulfabenzamide (SBA), sulfanitran (SNT), sulfasalazine (SSA), sulfamoxole (SXL), sulfisoxazole (SIZ), sulfamethoxazole (SMX), sulfaphenazole (SPA), sulfamethizole (SMT), sulfathiazole (STZ),

phthalylsulfathiazole (PST), sulfaguanidine (SG), sulfacetamide (SA), sulfanilamide (SN), uracil-5-sulfamic acid (SAU), *para*-aminobenzoic acid (PABA), trimethoprim (TMP), Diaveridin (DVD), and Bispyribac-sodium (BS) were purchased from Sigma-Aldrich (St. Louis, MO, USA) or Dr. Ehrenstorfer GmbH (Augsburg, Germany). Standards 2,4-dimethoxypyrimidin-5-amine (DM5A), 2,6-dimethoxypyrimidin-4-amine (DM4A), 2,4-dimethoxypyrimidine-5-carbaldehyde (DMC), 2-chloro-4,6-dimethoxypyrimidine (CDM), 1,3-dimethoxy-5-methylbenzene (DM), 2,4-dimethoxy pyrimidine (2DM), 4,6-Dimethoxypyrimidine (4DM), and Dimethoxymethane (DMT) were purchased from J&K Scientific (Beijing, China). Structure information of the above 42 standards is shown in Fig. 1A and Fig. 1B. LeukoLOCK total RNA isolation system, SuperScript III First-Strand Synthesis System, mouse mAb isotyping kit, and cell culture medium (DMEM) were purchased from ThermoFisher Scientific, Inc. (Waltham, MA, USA). SfiI, T4 DNA Ligase, and M13KO7 helper phage were purchased from New England Biolabs, Inc. (Ipswich, MA, USA). RNeasy Mini Kit, QIAquick Gel Extraction Kit, QIAquick PCR Purification Kit, and QIAGEN Plasmid Mini Kit were purchased from Qiagen, Inc. (Hilden, Germany). The vectors pAK100 and pJB33 were obtained as kind gifts from the Laboratory of Andreas Plückthun (Biochemisches Institut, Universität Zürich, Switzerland). High specific mouse mAb for SDM was obtained as a kind gift from the Laboratory of Hua Kuang (School of Food Science and Technology, Jiangnan University, Jiangsu, China). Our group produced rabbit anti-M13 IgG (H+L) and mouse anti-c-Myc tag IgG (H+L). Horseradish peroxidase (HRP)-conjugated goat anti-rabbit IgG (H+L), HRP-conjugated goat anti-mouse IgG (H+L), and HRP-conjugated goat anti-alpaca IgG (H+L) were purchased from Jackson ImmunoResearch Laboratories, Inc. (West Grove, PA, USA). Bovine Serum Albumin (BSA), ovalbumin (OVA), polyethylene glycol 8000 (PEG 8000), isopropyl-β-D-thiogalactopyranoside (IPTG), imidazole, hypoxanthine aminopterin thymidine (HAT), complete and incomplete Freund's adjuvant, polyethylene glycol 1500 (PEG 1500), and fetal calf serum were purchased from Sigma-Aldrich, Corp. (St. Louis, MO, USA). HisTrap HP, His tag protein purification column, was purchased from GE Healthcare Inc. (Marlborough, MA, USA). All other chemicals and solvents were of analytical grade or better and were obtained from Beijing Chemical Reagent Co., Ltd (Beijing, China).

2.2. Animals and Software

Two 4-year-old female alpacas were provided by Beijing Feiyaxin Co. Ltd. (Beijing, China). Female BALB/c mice were provided by Vital River Laboratory Animal Technology Co. Ltd. (Beijing, China). This work has received approval for research ethics from China Agricultural University and a proof/certificate of approval is available upon request.

Homologous modeling and molecular docking were conducted using Discovery Studio 2019 software (Dassault Systèmes, BIOVIA Corp., San Diego, CA, USA) and PyMOL software (Schrödinger, L. & DeLano, W., 2020. PyMOL, Available at: http://www.pymol.org/pymol).

2.3. Alpaca immunization and serum analysis

The immunogen SA10-X-BSA, the homologous coating antigen SA10-X-OVA, and the heterologous coating antigen TS-OVA were synthesized as previously described (Li et al., 2019; Wang et al., 2013). The hapten structure SA10-X is presented in Fig. 1C. Alpacas

were first immunized by subcutaneous injection of SA10-X-BSA (300 μg) diluted in 0.5 mL of phosphate-buffered saline (0.01 M PBS) mixed with 0.5 mL of Freund's complete adjuvant. Subsequent immunizations were completed with the same dose of antigen mixed with Freund's incomplete adjuvant (1:1 by volume) at 3-week intervals. Peripheral blood was collected before the first immunization and 1 week after each immunization. Antisera titers of each immunization were monitored by indirect enzyme-linked immunosorbent assay (i-ELISA) employing SA10-X-OVA as the coating antigen at a concentration of 0.1 μg/mL. The titer was defined as the dilution of antiserum that gives the optical density (OD) value of 1.5 at 450 nm. Antisera affinity to SDM was assessed by indirect competitive ELISA (ic-ELISA) employing TS-OVA as the coating antigen. The hapten structure TS is presented in Fig. 1C. For comparison, we also immunized mice with the same immunogen and prepared mouse mAb by hybridoma technology (Supplementary Material).

2.4. Library construction and selection

As shown in Fig. S1, total RNA was extracted from the peripheral blood lymphocytes using the LeukoLOCK total RNA isolation system. First-strand complementary DNA (cDNA) was derived from total RNA using the SuperScript III First-Strand Synthesis System. DNA fragments encoding the nanobodies were amplified by PCR using a set of primers with sfiI sites (Table S1). The PCR products were first purified using the QIAquick Gel Extraction Kit, then digested with sfiI restriction enzyme followed by purification with the QIAquick PCR Purification Kit. The final genes of nanobodies with two different sticky ends were ligated into the phagemid vector pAK100 by using T4 DNA ligase before transformation into electrocompetent *E. coli* XL1-Blue cells. After rescuing with M13KO7 helper phages, the nanobody repertoire was expressed as a pIII fusion protein on the surface of the phage. Finally, the resulting phage display library was harvested and purified by PEG8000/NaCl precipitation and then resuspended in PBS.

As shown in Fig. S1, the library (10^{12} transducing units) was subjected to five consecutive rounds of panning in 96-well microplates (Costar 2592, Corning). Table 1 lists the panning conditions of each round in this work. In the first round, one microplate strip was coated with 10 μg/mL of SA10-X-OVA (100 μL/well) overnight at 4°C and then blocked with 3% OVA in PBS (300 μL/well) for 2 h at 37°C. A pre-incubation of the library with 1.5% OVA is recommended to avoid the selection of OVA-binding phages. Then the blocked library was added to the microplate (100 μL/well) and incubated at 37°C for 1 h. After this, the microplate was washed fifteen times with PBST (0.05% Tween-20) and five times with PBS. Bound phages were eluted with Gly-HCl (0.2 M, pH 2.2,100 μL/well) and neutralized with Tris-HCl (2 M, pH 8.5, 20 μL/well). The plate counting method was used to control phage input in each round and calculate the output after panning, so as to judge whether the panning conditions were suitable. In the second round, bound phages were competitively eluted with 1000 μg/L SDM (100 μL/well) for 1 h under constant shaking at room temperature. In the third and fourth rounds, after coating (10 μg/mL and 1 μg/mL), blocking, binding, and washing, a mixture of the other 28 kinds of SAs (20 μg/L and 200 μg/L for each SAs) was added to the microplate and shaken for 1 h at room temperature. Phages eluted by these SAs were discarded while phages remaining in the microplate were finally eluted with SDM (1000 μg/L and 100 μg/L). In the fifth round, the microplate was

coated with 0.1 μg/mL of SA10-X-OVA, and phages were eluted with 10 μg/L of SDM. After each cycle of panning, the eluted phages were used to infect *E. coli* XL1-Blue cells for subsequent amplification and collection. Individual clones were picked randomly and tested by phage-ELISA. Phagemid DNAs derived from the positive phage clones were sequenced using primers shown in Table S1.

2.5. Nanobody expression and characterization

To express the nanobody free from the pIII peptide, the selected nanobody gene followed by a c-Myc tag was inserted in the pJB33 vector and then transformed into *E. coli* BL21(DE3). Individual colonies were selected from chloramphenicol (30 μg/mL) plates and amplified in Super Broth medium containing chloramphenicol at 37°C with shaking (220 rpm). Nanobody expression was induced by adding 0.5 mM of IPTG when the OD_{600nm} of the culture reached 0.8. After overnight growth at 25°C, cells were pelleted, and the periplasmic proteins were extracted by osmotic shock as described previously (Olichon et al., 2007). The purification of the nanobody was performed with a HisTrap HP His tag protein purification column in the AKTA purification system (GE Healthcare, Uppsala, Sweden) according to the manufacturer's instructions. The purity was assessed by running a 4%–12% sodium dodecyl sulfate-polyacrylamide gel electrophoresis (SDS−PAGE), stained with an eStain L1 Protein Staining System (GenScript, Nanjing, China).

Affinity.—For affinity determination, different concentrations of SDM and SA10-X-BSA ranging from 3.125 to 100 nM were added to a Series S Sensor Chip SA (GE Healthcare) to which ~2,000 RU of biotinylated nanobody had been coupled. All measurements were performed at 25°C using a flow rate of 30 μL/min in 0.2 M PB buffer (pH 5.3, 1% DMF). Different analyte concentrations are injected sequentially in a single cycle, with no regeneration between injections. All the data were processed using the Biacore 8K Evaluation software version 1.1.

Specificity.—The specificity of the nanobody was evaluated by determining the CR with the other 28 SAs and 13 structural analogs. For these studies, CR was calculated as CR (%) = (IC_{50} of SDM) / (IC_{50} of other analytes) × 100%.

Stability.—For the thermal stability study, the nanobody, as well as the rabbit polyclonal antibody (pAb) and mouse mAb, was incubated at 25°C, 30°C, 40°C, 50°C, 60°C, 70°C, 80°C, 90°C, and 100°C for 15 min. After cooling to room temperature, the samples were assayed for performance by ic-ELISA (Supplementary Material). Due to the excellent thermostability, the performance of the nanobody incubating at 100°C for 0, 5, 10, 15, 20, 25, and 30 min was evaluated, too. The melting temperature (T_m), aggregation temperature (T_{agg}), and hydrodynamic diameter (HD) of the nanobody were measured using the Unchained Labs Protein Stability Screening Platform (UNcle). Circular Dichroism (CD) was used to measure the corresponding spectrum and percentage of each secondary structure of the nanobody when gradually heated from 20°C to 100°C and then cooled to 25°C. For pH, ionic strength, and organic solvent stability study, the nanobody was diluted with 0.2 M PB at different pH values (4.0, 4.5, 5.0, 5.5, 6.0, 6.5, 7.0, 7.5, 8.0), different NaCl concentrations (0, 0.375, 0.75, 1.5, 3, 6 M), and different methanol concentrations (0, 5%, 10%, 15%, 20%,

25%, 30%, 35%, 40%, 45%, 50%). Then, the inhibition curves of ic-ELISA were generated at these conditions.

2.6. Homology modeling and molecular docking

The Discovery Studio 2019 (DS 2019, BIOVIA, CA, USA) computer program was used to construct the homology model of the nanobody. The Antibody Modeling Cascade protocol was used because it can build antibody models without requiring the light chain sequence. This protocol can automatically perform the following steps: 1. identify the antibody domains of the input sequence; 2. identify framework templates within the antibody database that contain the same domains and have the highest sequence similarity; 3. use the templates to build homology models for the framework regions; 4. identify complementarity-determining region (CDR) templates and use them to refine the CDR loop regions. The quality of the resulting model was evaluated by the Ramachandran Plot and Verify Protein (Profiles-3D) protocols. For protein-ligand docking, the 3D structure of SDM retrieved from the NCBI-PubChem compound database and the nanobody model obtained above were initialized as ligand molecule and receptor molecule using the Prepare Ligand and Prepare Protein tools, respectively. Then four CDR loops of nanobody were defined as binding sites, and the Dock Ligands (CDOCKER, CHARMm-based molecular dynamics) protocol was used to dock flexible SDM into a rigid nanobody binding site. All the generated ligand poses were evaluated by analyzing the interactions between SDM and nanobody from their 3D structures, 2D depictions, and property data. CDOCKER scores, which include internal ligand strain energy (-CDOCKER_ENERGY) and receptor-ligand interaction energy (-CDOCKER_INTERACTION_ENERGY), were also taken into consideration. According to the CR results and structural features of SDM, ligand poses with reasonable interactions and high CDOCKER scores were selected for further analysis.

2.7. Mutation verification and model calibration

Fourteen amino acids in the four CDR regions of H1–17 were considered as candidate key amino acids from the above docking poses and mutated to Ala for verification. The nanobody gene in the expression vector was mutated directly by using a Fast Mutagenesis System (TransGen Biotech, Beijing, China) following the manufacturer’s instructions. Then, the mutated express vector was sequenced and expressed to obtain the nanobody mutant as the procedures described above. The binding ability of the mutated nanobodies was evaluated by ic-ELISA. Based on the results, the nanobody structure was remodeled using the modeling protocol of an ordinary protein. The general procedure is basically the same as the Antibody Modeling Cascade except that every step of this protein modeling protocol is separate and can be controlled based on our purpose. Templates with similar characteristics to H1–17 were purposefully selected. CDR loop regions refinement was skipped because this step will remove the disulfide bond between C50 and C104. Finally, the model with two disulfide bonds, as well as the lowest Probability density function (PDF) total energy and low Discrete Optimized Protein Energy (DOPE) scores, was selected. Model evaluation and molecular docking were performed as described above. For comparison, we also prepared scFv from the mAb provided by Prof. Kuang and analyzed its recognition mechanism (Supplementary Material).

2.8. Sample preparation and recovery calculation

SDM-free river water samples and milk samples, including skimmed milk, low-fat milk, and whole milk samples were provided by the National Center for Veterinary Drug Safety Evaluation (Beijing, China). First, matrix interferences of water samples and different milk types were assessed by comparing the SDM standard curve prepared in milk with that prepared in assay buffer. Then the river sample and milk sample with the strongest matrix effect were chosen to reduce the matrix effect by diluting with PB buffers. To evaluate the accuracy and precision of the nanobody-based ic-ELISA, recovery studies were performed with SDM spiked samples (10, 20, and 40 μg/L in river water sample; 3, 6, and 12 μg/L in milk sample) without and with spiking other mixed SAs as the interference. Each spiked sample was analyzed in triplicate. The recoveries were calculated according to the standard curve and the following equation: Recovery (%) = [measured value (μg/L)] / [spiked value (μg/L)] × 100%. The limit of detection (LOD) was determined as the mean of the blank samples (n=20) plus 3SD.

3. Results and discussion

3.1. Analysis of antisera from alpaca and mouse

As shown in Fig. 1C, the general hapten of SA10-X was previously synthesized and characterized by our group (Li et al., 2019). It was initially designed to produce a broad-specific antibody to SAs since the SA10-X possesses the para-aminobenzenesulfonamide moiety at the far end of SAs and can maximally expose the common structure of SAs (Fig. 1C). Using the hapten SA10-X, we did obtain one broad-specific polyclonal antibody derived from rabbit recognizing 19 SAs with 50% inhibition (IC_{50}) below 100 μg/L (Li et al., 2019). Here, the reason we selected SA10-X rather than SDM as immunizing hapten was to prove that an ultra-specific antibody to a single SA could be obtained by phage display incorporating a counter-selection strategy, even if a general hapten is used. Before immunization, the hapten SA10-X was conjugated to BSA and identified by matrix-assisted laser desorption/ionization-time of flight mass spectrometry (MALDI-TOF MS) with a calculated hapten/BSA ratio of 7:1 (Fig. S2).

We used SA10-X-BSA to immunize not only alpaca for nanobody but also mouse for mAb to establish a fair comparison. Since a good immune response is a foundation for obtaining both nanobodies and mAbs, it is essential to monitor antisera before library construction and hybridoma preparation. After screening the antisera of the alpacas and mice, alpaca#1 and mouse#5 were selected for the subsequent experiment because of the higher titer and affinity of their antisera. As shown in Fig. 2A and Fig. 2B, a general trend of gradually increasing titer as immunization continued was seen in both alpaca#1 and mouse#5, reaching 2×10^5 and 5×10^4 after the fourth immunization, respectively. During the immunization period, the antibody titers of the alpaca were always higher than those of the mouse, implying a stronger immune response achieved by the alpaca.

We summarized the specificity of antisera to 29 SAs for alpaca#1 and mouse#5 in Table S2. It can be observed that the alpaca#1 antiserum could recognize at least 24 SAs, with IC_{50} ranging from 1.6 to 1509.2 μg/L, of which 7 SAs showed similar or better affinity

compared with SDM (IC_{50}: 5.4 μg/L). Meanwhile, the mouse#5 antiserum also could recognize 24 SAs, with IC_{50} ranging from 1.3 to 2722.5 μg/L, of which 6 SAs showed better affinity compared with SDM (IC_{50}: 16.6 μg/L). These results showed that the hapten SA10-X induced broad-specific antiserum responses in both alpaca and mouse, as previously observed with rabbit antisera (Li et al., 2019). The results indicated that it is not possible to obtain ultra-specific polyclonal antibodies to SDM in any species since the antisera are composed of the entire distribution of IgG antibodies with varying specificities (Jain and Salunke, 2019). Hybridoma or phage display technology could theoretically isolate any ultra-specific mAb from the antibody pool. Thus, we then prepared nanobodies and mAbs. Considering that the antiserum titer and affinity of the third and fourth immunizations did not change greatly for both alpaca and mouse (Fig. 2C), the alpaca#1 blood and mouse#5 spleen of the fourth immunization were collected for nanobody library construction and hybridoma preparation.

3.2. Isolation of SDM-specific nanobody

Phage display technology is a powerful tool for high-throughput screening of antibodies with the desired properties (Peltomaa et al., 2019). A single displayed antibody, even if not favored in the immune response, can be isolated precisely from a pool of billions of variants depending on the quality and execution of the designed selection procedure (Tabares-da Rosa et al., 2011). An immune phage display library of 5×10^6 individual nanobodies was constructed to select SDM-specific phages through five rounds of panning. The screening stringency was gradually increased by adding competitive elution, counter selection, and washing steps as well as adjusting the concentration of coating antigen, target, and counter selection analogs based on phage output and enrichment results (Table 1). To maximize phage capture and reduce the loss of nanobody diversity, a highly concentrated homologous coating antigen SA10-X-OVA, and the acid elution method was used in the first round of panning. In the second round, competitive elution by a high concentration of SDM was employed to ensure that the eluted phages could bind SDM. Obviously, many phages presented varied CR with other SAs according to the results of alpaca antiserum. To remove these phages, crucial counter selection and washing steps were designed in the third and fourth rounds of panning. Compared with the third round, the fourth round provided more stringent conditions by decreasing the concentration of SDM and increasing the concentration of interfering SAs, which was greatly beneficial to isolate more specific nanobodies to SDM. In addition to refining the specificity, it is also considered to improve the affinity by reducing the concentration of coating antigen and SDM in the fourth and fifth rounds of panning, which was conducive to the isolation of high affinity nanobodies. After the tightly controlled panning, a nanobody named H1–17 with ultra-specificity for SDM was successfully isolated. It is possible that the selective pressure was too strong because the H1–17 was highly enriched and was the only sequence present in the sequenced 16 clones (Fig. 2D).

Generally, it is difficult to obtain nanobodies with high affinity and specificity for chemical compounds, mainly because the molecular weights (< 1000 Da) of these hapten molecules are too small and some of them cannot even constitute one single epitope (Bever et al., 2016). Many reports provided panning strategies for hapten molecules, for example, using

a heterologous coating antigen was proved more efficient in the selection of a higher specific and affinity nanobody than using a homologous coating antigen (Wang et al., 2014). However, in this study, we failed to obtain any positive clones bind to SDM when employing one heterologous coating antigen TS-OVA, which performed well in the alpaca antiserum-based indirect competitive ELISA. Perhaps the binding between TS-OVA and phages was too weak to compete with other SAs during the counter selection panning or the desired phages cannot bind to TS-OVA due to its different structure from SDM. Our results showed that the panning procedure for hapten molecules involving heterologous antigen selection may bring a great risk of losing phage diversity and may not be suitable for counter selection strategies.

The isolated nanobody H1–17 with c-Myc tag and 6×His tag was inserted into the pJB33 vector via the sfiI restriction site (Fig. 2E) and expressed with a protein product yield of about 10 mg/L in soluble form in BL21 (DE3). The SDS-PAGE result of purified H1–17 with its characteristic band at 19 KD is shown in Fig. 2E. For comparison, we also prepared one mAb named 1D4 from mouse#5 after antisera screening using the standard hybridoma procedure (Supplementary Material).

3.3. Characterization of nanobody

The purified H1–17 was tested for its performance in terms of affinity, stability, and specificity by ic-ELISA and SPR. During the selection of coating antigen, it was found that H1–17 could not recognize any other heterologous coating antigens, including TS-OVA, SS-OVA, PB-OVA, BS-OVA, and HS-OVA (the structures of these haptens are shown in Fig. 1C), which once again proved that this nanobody cannot be obtained by using heterologous coating antigen selection strategy. Working concentrations of the homologous coating antigen (SA10-X-OVA, 0.1 μg/mL) and H1–17 (0.25 μg/mL) were chosen by checkerboard titration. Under the optimal conditions, the IC_{50} of H1–17 in the ic-ELISA to SDM was 1.1 μg/L, which was about five times better than that of the alpaca#1 antiserum (5.4 μg/L). Given the inferior position of heavy chain antibodies in alpaca antiserum and the high affinity of the obtained nanobody, it shows that reducing the concentrations of coating antigen and SDM in our panning strategy was effective for isolating high affinity nanobodies. We then compared the antibodies to SDM derived from different species immunized by the same SA10-X-BSA. As shown in Fig. 2F, the IC_{50} of H1–17 was about ten times better than that of the rabbit pAb (10.3 μg/L) in ic-ELISA (Li et al., 2019). Unfortunately, the obtained mAb1D4 recognized SDM with the IC_{50} value of above 10,000 μg/L, indicating that the standard hybridoma technology provided a low fusion ratio, and many specific clones were lost during the fusion procedure, especially in the case of hapten-specific mAbs. More importantly, the use of hybridoma technology to prepare mAbs sometimes fails to obtain the desired mAb for the analyte of interest such as SDM because it lacks the controlled panning procedure that is used in phage display (Puligedda et al., 2019).

Affinity.—We used SPR to test the interaction of H1–17 with SDM and SA10-X-OVA. The kinetic parameters, dissociation rate constants (k_d), association rate constants (k_a), and equilibrium dissociation constant (K_D) are presented in Table 2. The K_D values of H1–17 to SDM (1.05×10^{-9} M) and SA10-X-OVA (3.33×10^{-9} M) were comparable and in the

nanomolar range. However, the k_a and k_d values of SDM and SA10-X-OVA were different by about one- or two-order of magnitude, for example, 1.29×10^6 1/Ms *vs.* 5.25×10^4 1/Ms in the case of k_a, 1.36×10^{-3} 1/s *vs.* 1.75×10^{-4} 1/s in the case of k_d. In our previous study, two broad-spectrum anti-SAs mouse mAbs, named 4C7 and 4D11, were obtained, and their kinetic parameters with SDM were also listed in Table 2 for comparison (Li et al., 2019). As can be seen from Table 2, the k_a between H1–17 and SDM was overwhelmingly dominant compared to other antibodies or analyte. The k_a and k_d between H1–17 and SA10-X-OVA were at medium levels. This moderate dissociation rate not only makes H1–17 less easily eluted by the other 28 competitive SAs during the counter selection step but also allows H1–17 to be eluted by SDM due to the faster association rate between H1–17 and SDM.

Specificity.—The IC_{50} values of H1–17 in the ic-ELISA were tested by 29 SAs (Fig. 1A) and 13 structurally similar analytes (Fig. 1B). The negative CR values (<0.1%) of all 41 compounds tested confirmed the ultra-specificity of H1–17 for SDM. Fig. 3 shows a bar graph that compares 29 SAs CR values of rabbit serum, alpaca#1 serum, nanobody H1–17 from alpaca#1, mouse#5 serum, mAb1D4 from mouse#5, and mouse mAb from Prof. Kuang (Kuang et al., 2013). The detailed IC_{50} and CR values are shown in Table S2. All the antibodies were induced by the same immunizing hapten SA10-X except mAb from Prof. Kuang which was induced directly by SDM as the immunizing hapten. From Fig. 3, we can see that all the pAbs (serum) had broad specificity and the mAb1D4 could recognize four SAs, while H1–17 (colored green) is distinguished by its ultra-specificity from other antibodies. Surprisingly, the mAb from Prof. Kuang, which was supposed to recognize SDM with high specificity and actually has high CR values with sulfaquinoxaline (SQX, 19.1%), and observable CRs with sulfamonomethoxine (SMM, 1.6%) and sulfachlorpyrazine (SCY, 1.5%). These results demonstrated that H1–17 possesses higher specificity than any other conventional antibodies, regardless of whether these conventional antibodies were induced by the same general hapten or by the appropriate hapten structure of the target analyte.

Stability.—Stability is one of the most extraordinary features of nanobodies (Muyldermans, 2013). We conducted a series of tolerance evaluations for H1–17, including thermal, pH, ionic strength, and organic solvent. In Fig. 4A, we observed that the binding activity of H1–17 was kept above 80% after heating for 15 min at temperatures ranging from 30°C to 100°C, while that of mAb1D4 and rabbit pAb declined rapidly when the temperature is above 60°C and 70°C, respectively, showing that H1–17 possesses excellent thermal stability compared to pAb and mAb1D4 counterparts. In particular, standard curves of ic-ELISA based on H1–17 for SDM were constructed after incubating at 100°C for different times (Fig. 4B). The results show that there is no significant decrease in IC_{50} values (0.76–1.29 μg/L) even after heating H1–17 at 100°C for 30 min. To further analyze the thermal stability of H1–17, fluorescence, static light scattering (SLS), and dynamic light scattering (DLS) were used to measure other thermal stability parameters. Results show that the T_m value of H1–17 was 72.0°C, the T_{agg} value of H1–17 was 70.7°C, the particle size distribution of H1–17 in the PBS buffer was uniform, the average HD was 3.9 nm (Fig. 4C). Since H1–17 has excellent heat resistance but not very high T_m and T_{agg} values, it may be refolded after heating to restore its binding ability. This speculation was confirmed by the subsequent CD spectroscopy results. Fig. 4D shows an obvious CD spectrum change of H1–

17 upon gradual heating from 20°C (green) to 100°C (red). The CD spectrum of H1–17 was restored when cooled back to room temperature (25°C, blue), although not to its original state, which appeared to be sufficient for antigen binding. Fig. 4E shows the quantitative analysis results of the secondary structure of H1–17. As the temperature increases (green to red), the proportions of the helix, beta-turn, and random coil (Rndm.Coil) tend to increase, while antiparallel and parallel tend to decrease. When cooled to room temperature (blue), the proportions of all types of secondary structures recovered to varying degrees. In addition to excellent thermal stability, H1–17 showed good tolerance to the environment of low pH (Fig. 4F), ionic strength in the range of 0–6 M (Fig. 4G), and up to 50% methanol (Fig. 4H). The high stability of H1–17 is advantageous for applications with real samples.

3.4. Analysis of the recognition mechanism of nanobody

To study the structural mechanism of the ultra-specificity of H1–17, we constructed the nanobody structure and performed a docking study by molecular simulation that was then verified by mutation experiments. At first, the model of H1–17 was built by an automatic modeling process of DS 2019 which choose templates simply based on sequence similarity. After model quality evaluation and flexible docking with SDM from all the possible binding sites of the CDRs (Fig. 5A), 14 amino acids were selected as candidate key amino acids and mutated to Ala for verification (Fig. 5B). In Fig. 5C we can see that the binding ability of mutants C104A and Y106A was significantly decreased, indicating that the most probable binding site of H1–17 is located in the CDR3 region, and the binding event may be related to the noncanonical disulfide bond (C50-C104) of the nanobody (Saerens et al., 2008). To evaluate this hypothesis, we cleaved the disulfide bond by mutating C50 to Ala and found that the binding ability of H1–17 was lost entirely due to the structural collapse, indicating that the noncanonical disulfide bond did exit and played a critical role in the binding of SDM (Fig. 5D). On the contrary, the mutation of C22 and C96, which are conserved to form the conventional disulfide bond, did not influence the binding ability of H1–17 to SDM (Fig. 5D) and that was consistent with the previous report (Liu et al., 2019). Since the noncanonical disulfide bond was not formed in the nanobody model obtained using only highly similar sequences templates, templates with high sequence identity, comparable CDRs lengths, and similar Cys positions were purposefully selected during the remodel of H1–17 (Fig. S3A). Model evaluation results of Ramachandran Plot and Profiles-3D in Fig. S3B and Fig. S3C indicate that the H1–17 model is of high quality. Through the above studies, we obtained a more accurate 3D spatial model and confirmed the binding site location of H1–17 (Fig. 5E). We also aligned the former and the new model in Fig. 5F and found that the noncanonical disulfide bond formed between C50 and C104 bends the CDR3 loop towards the interior of the nanobody in the new model, forming a stable binding cavity. The new model of H1–17 is more credible according to the mutation experiment, and the docking experiment was then conducted based on this model.

It can be observed in Fig. 6A that SDM was half surrounded in the tailor-made binding pocket formed by CDR3 (red), FR2 (gray), and the critical noncanonical disulfide bond (magenta). The disulfide bond formed by C50 and C104 divides the binding pocket into a deep narrow bottom and a shallow wide edge to perfectly accommodate SDM. The methoxyl at the C-6 position of the pyrimidine ring was deeply embedded in the

narrow bottom of the pocket when the C-2 methoxyl of the pyrimidine ring pointed outward. The common substructure of SAs, the para-aminobenzenesulfonamide moiety, was exposed on the wide edge of the pocket. Fig. 6B shows the interactions between SDM and H1–17, including hydrogen bonds (green, C104, and Y106), π-anion (yellow, Y106), π-sulfur (orange, F37), and hydrophobic force (pink, π-π T-shaped from F37 and Y106, amide-π stacked from C104, and π-alkyl from C50, C104, and A108) interactions. Detailed information about the interactions is shown in Table S3. Since H1–17 could not recognize sulfisomidine (SIM), 2,6-dimethoxypyrimidin-4-amine (DM4A), and 2,4-dimethoxypyrimidine (2DM) in Fig. 1A and Fig. 1B (colored blue), in the authors' opinion, the ultra-specificity of the nanobody was mainly attributed to the two hydrogen bonds between C104 and the oxygen on the C-6 methoxyl of the pyrimidine ring and between Y106 and the oxygen on the sulfonyl of the para-aminobenzenesulfonamide moiety. These two hydrogen bonds form a fixed angle at the bottom and the edge of the binding pocket, like a pair of mutual-checking partners, co-verification the target molecule. Therefore, either the analog lacks the common structure of SAs or the feature C-6 methoxyl of SDM, they cannot bind to H1–17.

To study the difference in the recognition mechanism between the nanobody and the conventional antibody, we prepared scFv from the mAb provided by Prof. Kuang (Supplementary Material). The scFv model and evaluation results are displayed in Fig. S4, indicating that the model is of high quality. Compare to H1–17, the binding pocket of scFv was flat and wide (Fig. 6C) which made it easier to accommodate other SAs (Fig. S5). As shown in Fig. 6D and Table S4, there is a key hydrogen bond between L-Y42 and the hydrogen on the C-6 methoxyl of the pyrimidine ring, ensuring the specificity of scFv; however, it can be observed that most interaction forces between SDM and scFv, including the other three hydrogen bonds, were formed between scFv and the para-aminobenzenesulfonamide moiety, which may result in the binding to other SAs. To sum up, due to the noncanonical disulfide bond, H1–17 has both a tailor-made binding pocket and mutual-checking hydrogen bonds, which lead to its higher specificity than scFv.

There are five small molecules have been crystallized in complex with their corresponding nanobodies in the PDB, namely azo-dye reactive red 6 (RR6), azo-dye reactive red 1 (RR1), methotrexate (MTX), triclocarban (TCC), and cortisol, whose binding mode can be divided into two types (Spinelli et al., 2000; Spinelli et al., 2001; Fanning and Horn, 2011; Tabares Da Rosa et al., 2019; Ding et al., 2019). One is similar to that of the four-chain antibody by the conventional binding mode (Fig. S6A, S6B), which usually needs the joint contribution of CDR2 and/or CDR1 in addition to CDR3 (Spinelli et al., 2000; Spinelli et al., 2001). In the other, which is called CDR1 tunneling mode and is unique to nanobodies (Fig. S6C–E), the small molecule binds in an under-loop tunnel formed by CDR1 and contacts with CDR4 (Fanning and Horn, 2011; Tabares Da Rosa et al., 2019; Ding et al., 2019). We have compared these complexes with H1–17-SDM in Fig. S7 and Table 3, including the alignment of sequences and structures, the length of CDR1–4, the number (location) of cysteines, and the number of disulfide bonds. It seems that nanobodies prefer to bind bigger molecules (RR6, RR1 >500 Da) by the conventional binding mode and to smaller molecules by the CDR1 tunneling mode (MTX, TCC, Cortisol < 500 Da) (Ding et al., 2019). In the study, however, the smallest molecule SDM (310.33 Da) binding to H1–17 did

not follow these two modes. One novel binding mode for nanobodies and small molecules, CDR3 plus the noncanonical disulfide bond, was discovered (Fig. S6F). In this mode, the binding of SDM to the nanobody was mainly dependent on CDR3 and the noncanonical disulfide bond without involving any other CDRs. Since the length of CDR3 of H1–17 is shorter compared with other nanobodies (Fig. S7), the noncanonical disulfide bond may be a necessary complement to the lack of CDR3 length to form the smaller binding cavity that mainly contributed to the ultra-specificity of the H1–17.

3.5. Performance of nanobody in real sample analysis

The extensive use of SDM has resulted in its residues in the environment and animal-derived food, so we selected river water and milk samples for spiked sample analysis. Due to the complex composition of the environmental sample, the river water samples require a 10-fold dilution with PB buffer (0.02 M, pH 4.5) to eliminate matrix effects (Fig. S8A). Milk is considered a highly challenging matrix because of its complex composition. In general, matrix effects vary according to the fat content of milk (Zacco et al., 2007). In this study, skimmed milk, low-fat milk, and whole milk were used to evaluate the influence of the matrix on the H1–17-based ic-ELISA. As shown in Fig. S8B, there was no obvious relationship between fat content and matrix effect. The strongest matrix effects of whole milk sample 6 could be successfully reduced by four times dilution with PB buffer (0.02 M, pH 4.5) (Fig. S8C). The LODs of the ic-ELISA in the river water and whole milk samples were calculated to be 1.28 μg/L and 0.76 μg/L, respectively. The developed ic-ELISA was then used to quantify samples spiked with SDM and the recoveries and coefficients of variation (CV) are listed in Table 4. It shows recoveries in the river sample were between 94.6%−106.1% with CVs below 9.2% and recoveries in the milk sample were between 100.2%−114% with CVs below 12.7%. Besides, the results were not affected by adding other SAs as interferences. This demonstrates that the H1–17-based ic-ELISA satisfies the requirements for a screening detection method and can be used for SDM residue measurement in the river and milk samples with a low false positive rate.

4. Conclusions

This study demonstrates nanobodies can reach ultra-specificity by a well-designed isolation strategy and illuminates the relationship between the ultra-specificity and the unique structure of nanobodies. Taking SDM as a model molecule, we improved the false positive problem in immunoassay by preparing ultra-specific nanobodies. Owing to the homologous antigen counter selection strategy, the nanobody H1–17 we obtained is by far the most specific SDM antibody with nanomolar affinity and excellent stability, which makes the immunoassay robust and low false positive rate. The recognition mechanism study revealed the noncanonical disulfide bond between FR2 and CDR3 of the nanobody plays a significant role in both binding site conformation and intermolecular interactions, which not only explained the ultra-specificity of H1–17 but also provided useful information for further development and optimization of antibodies. Taking the many advantages of nanobodies into consideration, these ultra-specific nanobodies constitute a powerful tool for the development of high-quality immunoassays for chemical compounds in the field of environmental pollutants monitoring, food safety analysis, and clinical diagnostics.

Supplementary Material

Refer to Web version on PubMed Central for supplementary material.

Acknowledgments

This work was supported by the China Postdoctoral Science Foundation (2021M703526), the National Natural Science Foundation of China (31902325 and 31873025), the China Agriculture Research System (CARS-36), and the National Institutes of Environmental Health Sciences Superfund Research Program (P42ES04699). The authors thank Prof. Kuang for providing the anti-SDM mAb.

References

Baker M, 2015. Reproducibility crisis: blame it on the antibodies. Nature 521, 274–276. [PubMed: 25993940]

Ben Y, Hu M, Zhang X, Wu S, Wong MH, Wang M, Andrews CB, Zheng C, 2020. Efficient detection and assessment of human exposure to trace antibiotic residues in drinking water. Water Res. 175, 115699. [PubMed: 32200333]

Bever CS, Dong J, Vasylieva N, Barnych B, Cui Y, Xu Z, Hammock BD, Gee SJ, 2016. VHH antibodies: emerging reagents for the analysis of environmental chemicals. Anal. Bioanal. Chem 408 (22), 5985–6002. [PubMed: 27209591]

Bordeaux J, Welsh AW, Agarwal S, Killiam E, Baquero MT, Hanna JA, Anagnostou VK, Rimm DL, 2010. Antibody validation. Biotechniques 48 (3), 197–209. [PubMed: 20359301]

Bradbury A, Plückthun A, 2015. Standardize antibodies used in research. Nature 518, 27–29. [PubMed: 25652980]

Bradbury ARM, Trinklein ND, Thie H, Wilkinson IC, Tandon AK, Anderson S, Bladen CL, Jones B, Aldred SF, Bestagno M, Burrone O, Maynard J, Ferrara F, Trimmer JS, Görnemann J, Glanville J, Wolf P, Frenzel A, Wong J, Koh XY, Eng H, Lane D, Lefranc M, Clark M, Dübel S, 2018. When monoclonal antibodies are not monospecific: hybridomas frequently express additional functional variable regions. MAbs-Austin 10 (4), 539–546.

Deckers N, Saerens D, Kanobana K, Conrath K, Victor B, Wernery U, Vercruysse J, Muyldermans S, Dorny P, 2009. Nanobodies, a promising tool for species-specific diagnosis of Taenia solium cysticercosis. Int. J. Parasitol 39 (5), 625–633. [PubMed: 19041315]

Ding L, Wang Z, Zhong P, Jiang H, Zhao Z, Zhang Y, Ren Z, Ding Y, 2019. Structural insights into the mechanism of single domain VHH antibody binding to cortisol. FEBS Letters 593 (11), 1248–1256. [PubMed: 31049949]

Egelhofer TA, Minoda A, Klugman S, 2011. An assessment of histone-modification antibody quality. Nat. Struct. Mol. Biol 18 (1), 91–93. [PubMed: 21131980]

Fanning SW, Horn JR, 2011. An anti-hapten camelid antibody reveals a cryptic binding site with significant energetic contributions from a nonhypervariable loop. Protein Sci. 20 (7), 1196–1207. [PubMed: 21557375]

Genst ED, Silence K, Decanniere K, Conrath K, Loris R, Kinne J, Muyldermans S, Wyns L, 2006. Molecular basis for the preferential cleft recognition by dromedary Heavy-Chain antibodies. P. Natl. Acad. Sci. USA 103 (12), 4586–4591.

Hamers-Casterman C, Atarhouch T, Muyldermans S, Robinson G, Hamers C, Songa EB, Bendahman N, Hamers R, 1993. Narurally occurring antibodies devoid of light chains. Nature 363, 446–448. [PubMed: 8502296]

He J, Ma S, Wu S, Xu J, Tian J, Li J, Gee SJ, Hammock BD, Li QX, Xu T, 2020. Construction of immunomagnetic particles with high stability in stringent conditions by site-directed immobilization of multivalent nanobodies onto bacterial magnetic particles for the environmental detection of tetrabromobisphenol-A. Anal. Chem 92 (1), 1114–1121. [PubMed: 31763820]

Huang F, An Z, Moran MJ, Liu F, 2020. Recognition of typical antibiotic residues in environmental media related to groundwater in China (2009−2019). J. Hazard. Mater 399, 122813. [PubMed: 32937691]

Ingram JR, Schmidt FI, Ploegh HL, 2018. Exploiting nanobodies' singular traits. Annu. Rev. Immunol 36, 695–715. [PubMed: 29490163]

Jain D, Salunke DM, 2019. Antibody specificity and promiscuity. Biochem. J 476 (3), 433–447. [PubMed: 30723137]

Kuang H, Chen X, Hao C, Ma W, Xu L, Xu C, 2013. Immuno-driven plasmonic oligomer sensor for the ultrasensitive detection of antibiotics. RSC Adv. 3 (38), 17294–17299.

Landsteiner K, 2013. The Specificity of Serological Reactions. Revised ed. Courier Corporation.

Li B, Wu D, Li Y, Shi Y, Wang C, Sun J, Song C, 2022. Metabolic mechanism of sulfadimethoxine biodegradation by Chlorella sp. L38 and Phaeodactylum tricornutum MASCC-0025. Front. Microbiol 13.

Li C, Liang X, Wen K, Li Y, Zhang X, Ma M, Yu X, Yu W, Shen J, Wang Z, 2019. Class-specific monoclonal antibodies and dihydropteroate synthase in bioassays used for the detection of sulfonamides: structural insights into recognition diversity. Anal Chem 91, 2392–2400. [PubMed: 30580515]

Li C, Luo X, Li Y, Yang H, Liang X, Wen K, Cao Y, Li C, Wang W, Shi W, Zhang S, Yu X, Wang Z, 2019. A Class-Selective immunoassay for sulfonamides residue detection in milk using a superior polyclonal antibody with broad specificity and highly uniform affinity. Molecules 24 (3), 443. [PubMed: 30691168]

Li C, Tang Z, Hu Z, Wang Y, Yang X, Mo F, Lu X, 2018. Natural single-domain antibody-nanobody: a novel concept in the antibody field. J. Biomed. Nanotechnol 14 (1), 1–19. [PubMed: 29463363]

Liu H, Schittny V, Nash MA, 2019. Removal of a conserved disulfide bond does not compromise mechanical stability of a VHH antibody complex. Nano Lett. 19 (8), 5524–5529. [PubMed: 31257893]

Michel MC, Wieland T, Tsujimoto G, 2009. How reliable are G-protein-coupled receptor antibodies. N.-S. Arch. Pharmacol 379, 385–388.

Muldoon MT, Holtzapple CK, Deshpande SS, Beier RC, Stanker LH, 2000. Development of a monoclonal Antibody-Based cELISA for the analysis of sulfadimethoxine. 1. Development and characterization of monoclonal antibodies and molecular modeling studies of antibody recognition. J. Agr. Food Chem 48 (2), 537–544. [PubMed: 10691672]

Muyldermans S, 2013. Nanobodies: Natural single-domain antibodies. Annu. Rev. Biochem 82, 775–797. [PubMed: 23495938]

Muyldermans S, Baral TN, Retamozzo VC, De Baetselier P, De Genst E, Kinne J, Leonhardt H, Magez S, Nguyen VK, Revets H, Rothbauer U, Stijlemans B, Tillib S, Wernery U, Wyns L, Hassanzadeh-Ghassabeh G, Saerens D, 2009. Camelid immunoglobulins and nanobody technology. Vet. Immunol. Immunop 128 (1–3), 178–183.

Olichon A, Schweizer D, Muyldermans S, de Marco A, 2007. Heating as a rapid purification method for recovering correctly-folded thermotolerant VH and VHH domains. BMC Biotechnol. 7 (1), 7. [PubMed: 17257422]

Peltomaa R, Benito-Peña E, Barderas R, Moreno-Bondi MC, 2019. Phage display in the quest for new selective recognition elements for biosensors. ACS Omega 4 (7), 11569–11580. [PubMed: 31460264]

Peveler WJ, Yazdani M, Rotello VM, 2016. Selectivity and specificity: Pros and cons in sensing. ACS Sensors 1 (11), 1282–1285. [PubMed: 30294676]

Prassas I, Diamandis EP, 2014. Translational researchers beware! Unreliable commercial immunoassays (ELISAs) can jeopardize your research. Clin. Chem. Lab. Med 52 (6), 765–766. [PubMed: 24497227]

Puligedda RD, Puligedda RD, Sharma R, Al-Saleem FH, Kouiavskaia D, Velu AB, Velu AB, Kattala CD, Kattala CD, Prendergast GC, Lynch DR, Chumakov K, Chumakov K, Dessain SK, Dessain SK, 2019. Capture and display of antibodies secreted by hybridoma cells enables fluorescent on-cell screening. MAbs-Austin 11 (3), 546–558.

Saerens D, Conrath K, Govaert J, Muyldermans S, 2008. Disulfide bond introduction for general stabilization of immunoglobulin Heavy-Chain variable domains. J. Mol. Biol 377 (2), 478–488. [PubMed: 18262543]

Spinelli S, Frenken LGJ, Hermans P, Verrips T, Brown K, Tegoni M, Cambillau C, 2000. Camelid heavy-chain variable domains provide efficient combining sites to haptens. Biochemistry-US 39 (6), 1217–1222.

Spinelli S, Tegoni M, Frenken L, van Vliet C, Cambillau C, 2001. Lateral recognition of a dye hapten by a llama VHH domain. J. Mol. Biol 311 (1), 123–129. [PubMed: 11469862]

Stijlemans B, Conrath K, Cortez-Retamozo V, Van Xong H, Wyns L, Senter P, Revets H, De Baetselier P, Muyldermans S, Magez S, 2004. Efficient targeting of conserved cryptic epitopes of infectious agents by single domain antibodies. J. Biol. Chem 279 (2), 1256–1261. [PubMed: 14527957]

Tabares-Da Rosa S, Wogulis LA, Wogulis MD, González Sapienza G, Wilson DK, 2019. Structure and specificity of several triclocarban-binding single domain camelid antibody fragments. J. Mol. Recognit 32 (1), e2755. [PubMed: 30033524]

Tabares-Da Rosa S, Rossotti M, Carleiza C, Carrión F, Pritsch O, Ahn KC, Last JA, Hammock BD, González-Sapienza G, 2011. Competitive selection from single domain antibody libraries allows isolation of high-affinity antihapten antibodies that are not favored in the llama immune response. Anal. Chem 83 (18), 7213–7220. [PubMed: 21827167]

The Japan Food Chemical Research Foundation, 2006. Residue Limits of Agricultural Chemicals.

Wang J, Bever CRS, Majkova Z, Dechant JE, Yang J, Gee SJ, Xu T, Hammock BD, 2014. Heterologous antigen selection of camelid heavy chain single domain antibodies against tetrabromobisphenol A. Anal. Chem 86 (16), 8296–8302. [PubMed: 25068372]

Wang Z, Beier RC, Sheng Y, Zhang S, Jiang W, Wang Z, Wang J, Shen J, 2013. Monoclonal antibodies with group specificity toward sulfonamides: selection of hapten and antibody selectivity. Anal. Bioanal. Chem 405 (12), 4027–4037. [PubMed: 23417550]

Wild D, 2013. The immunoassay handbook: Theory and applications of ligand binding, ELISA and related techniques. Fourth Edition. Elsevier Science.

Yang L, Ni H, Li C, Zhang X, Wen K, Ke Y, Yang H, Shia W, Zhang S, Shen J, Wang Z, 2019. Development of a highly specific chemiluminescence aptasensor for sulfamethazine detection in milk based on in vitro selected aptamers. Sensor. Actuat. B-Chem 281, 801–811.

Zacco E, Adrian J, Galve R, Marco MP, Alegret S, Pividori MI, 2007. Electrochemical magneto immunosensing of antibiotic residues in milk. Biosens. Bioelectron 22 (9–10), 2184–2191. [PubMed: 17126544]

Zhang J, Wang Y, Dong J, Yang J, Zhang Y, Wang F, Si R, Xu Z, Wang H, Xiao Z, Shen Y, 2019. Development of a simple pretreatment immunoassay based on an organic solvent-tolerant nanobody for the detection of carbofuran in vegetable and fruit samples. Biomolecules 9 (10), 576. [PubMed: 31591300]

Zhuang J, Wang S, Tan Y, Xiao R, Chen J, Wang X, Jiang L, Wang Z, 2019. Degradation of sulfadimethoxine by permanganate in aquatic environment: Influence factors, intermediate products and theoretical study. Sci. Total Environ 671, 705–713. [PubMed: 30939323]

Highlights

- A novel homologous antigen counter selection strategy was proposed for ultra-specific nanobody isolation.
- A nanobody with ultra-specificity to sulfadimethoxine was obtained.
- The specificity origin of nanobody was illuminated by molecular simulation and site-directed mutagenesis.
- A novel binding mode of nanobodies and small molecules was found.
- An immunoassay with a low positive rate was developed for sulfadimethoxine.

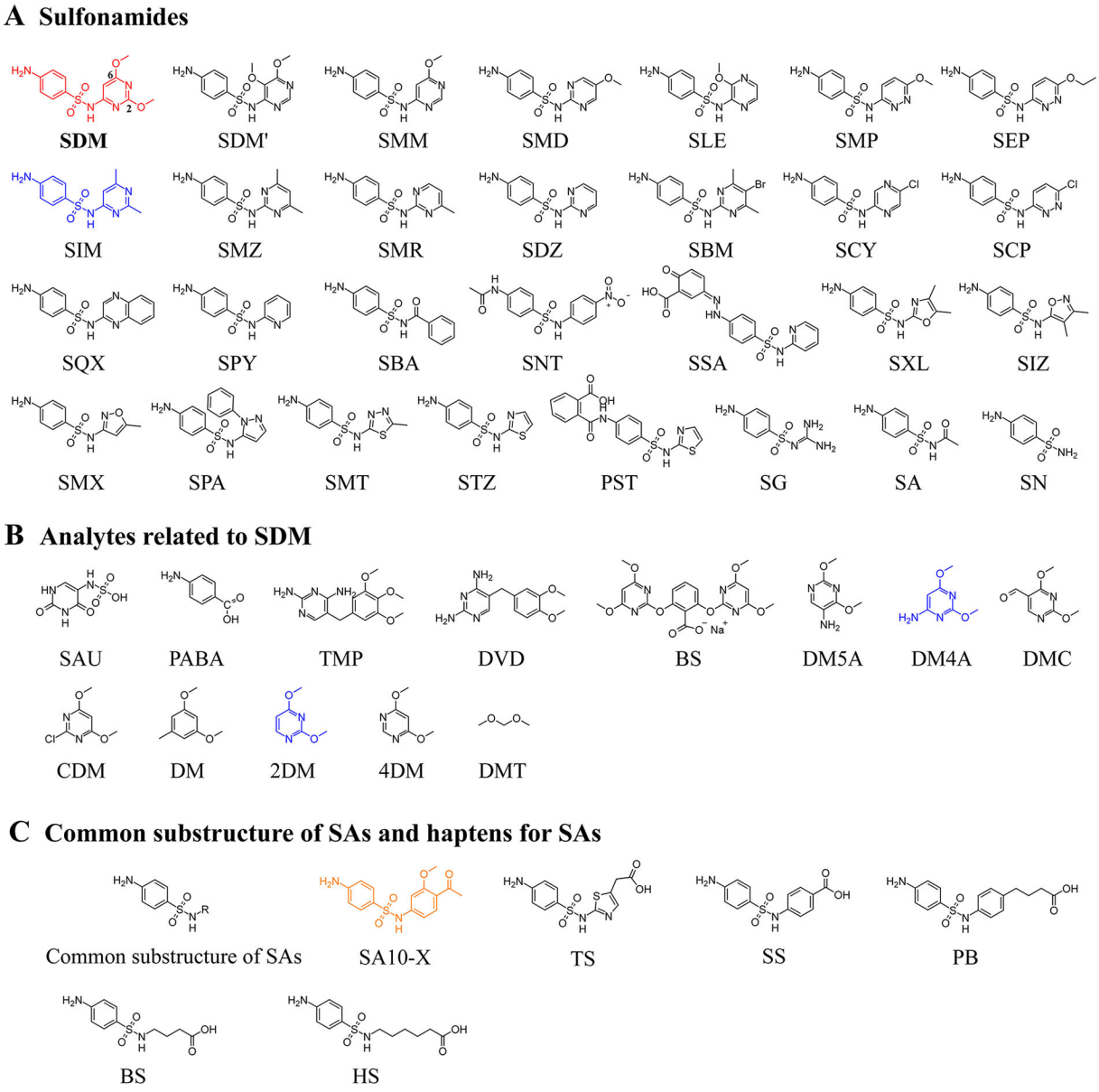

Fig. 1.

(A) Chemical structure of 29 SAs. The methoxyl group is labeled as number 2 and number 6 in the red SDM molecule. (B) Thirteen of structurally similar analytes related to SDM (C) Common substructure of SAs and the haptens for SAs. The orange hapten SA10-X is used to synthesize the immunogen and the analogs mentioned in the recognition mechanism study are colored blue.

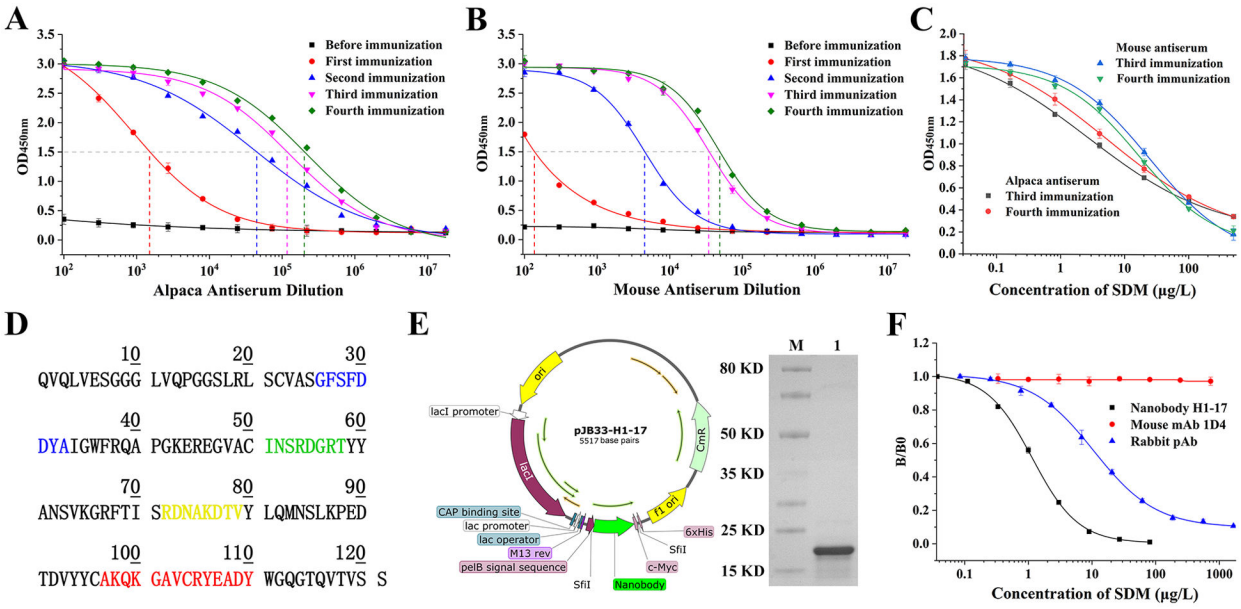

Fig. 2.

(A) Antisera titer of alpaca#1. (B) Antisera titer of mouse#5. (C) Antisera affinity of alpaca#1 and mouse#5. (D) The amino acid sequence of H1–17. CDR1, CDR2, CDR3, and CDR4 are colored blue, green, red, and yellow, respectively. (E) Recombinant expression plasmid map of pJB33-H1–17 (left) and SDS-PAGE result of the purified H1–17 (right). (F) Inhibition curves of SDM in H1–17, mouse mAb 1D4, and rabbit pAb-based ic-ELISA.

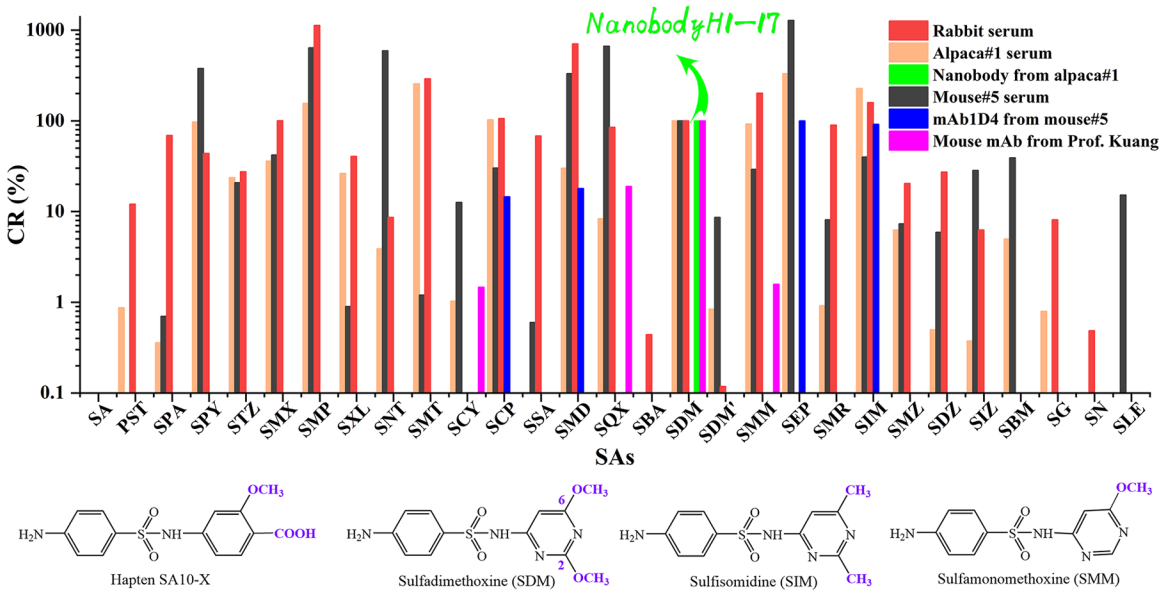

Fig. 3.

The CR values of different antibodies. Rabbit serum, alpaca#1 serum, nanobody H1–17, mouse#5 serum, mAb1D4, and mouse mAb from Prof. Kuang are colored red, orange, green, black, blue, and magenta, respectively. Structures of hapten, SDM, and similar SAs are shown below the bar graph.

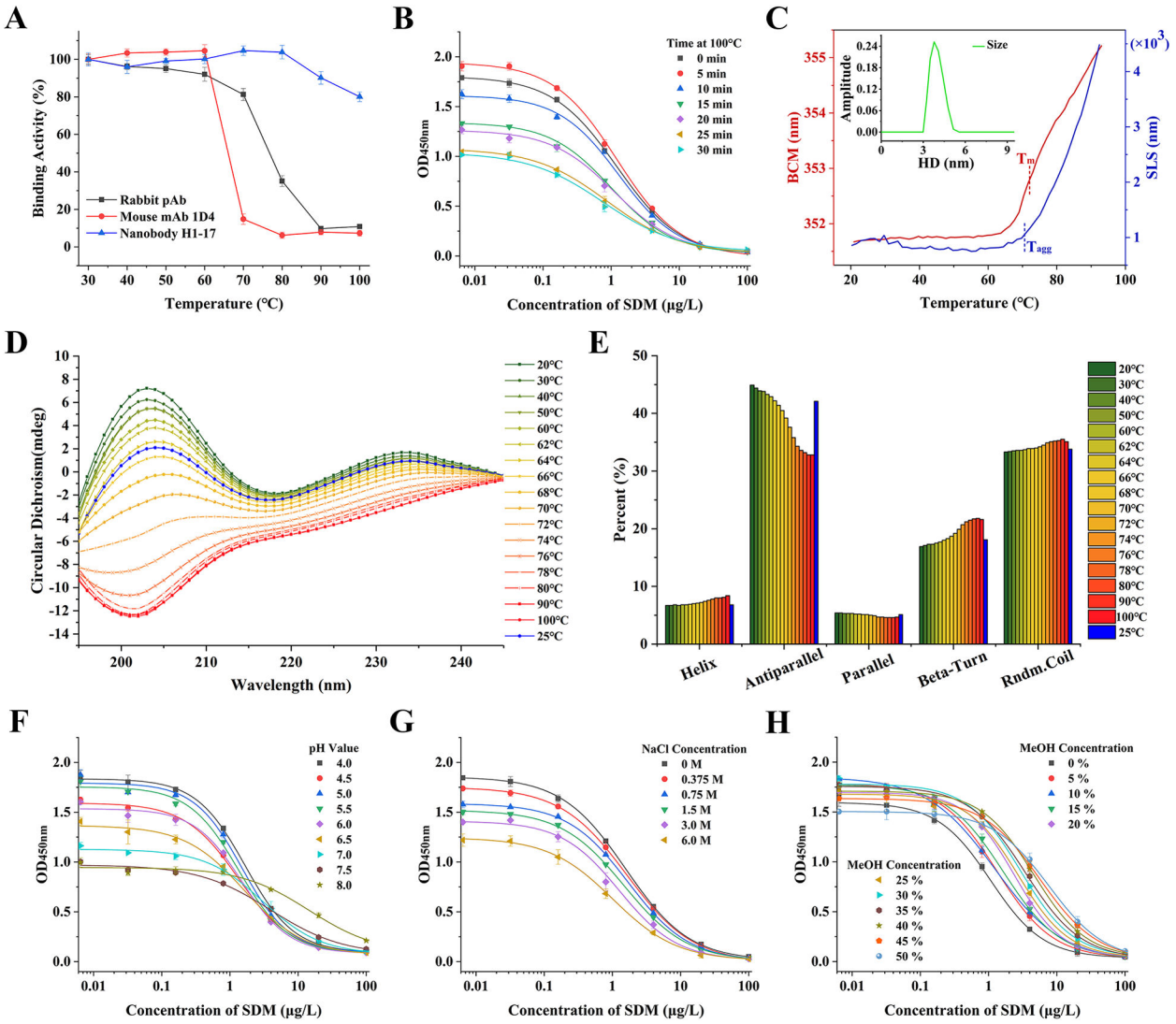

Fig. 4.

Stability characterization results of H1–17. (A) Binding activity of rabbit pAb, mAb 1D4, and H1–17 after 15 min treatment at different temperatures. (B) Thermal stability of H1–17 at 100°C. (C) T_m, T_{agg}, and HD values of H1–17 measured using fluorescence, SLS, and DLS. CD spectrum (D) and percentage of each secondary structure (E) of H1–17 when gradually heated from 20°C to 100°C and then cooled to 25°C. Effects of pH (F), NaCl (G), and methanol (H) on the performance of the H1–17-based ic-ELISA.

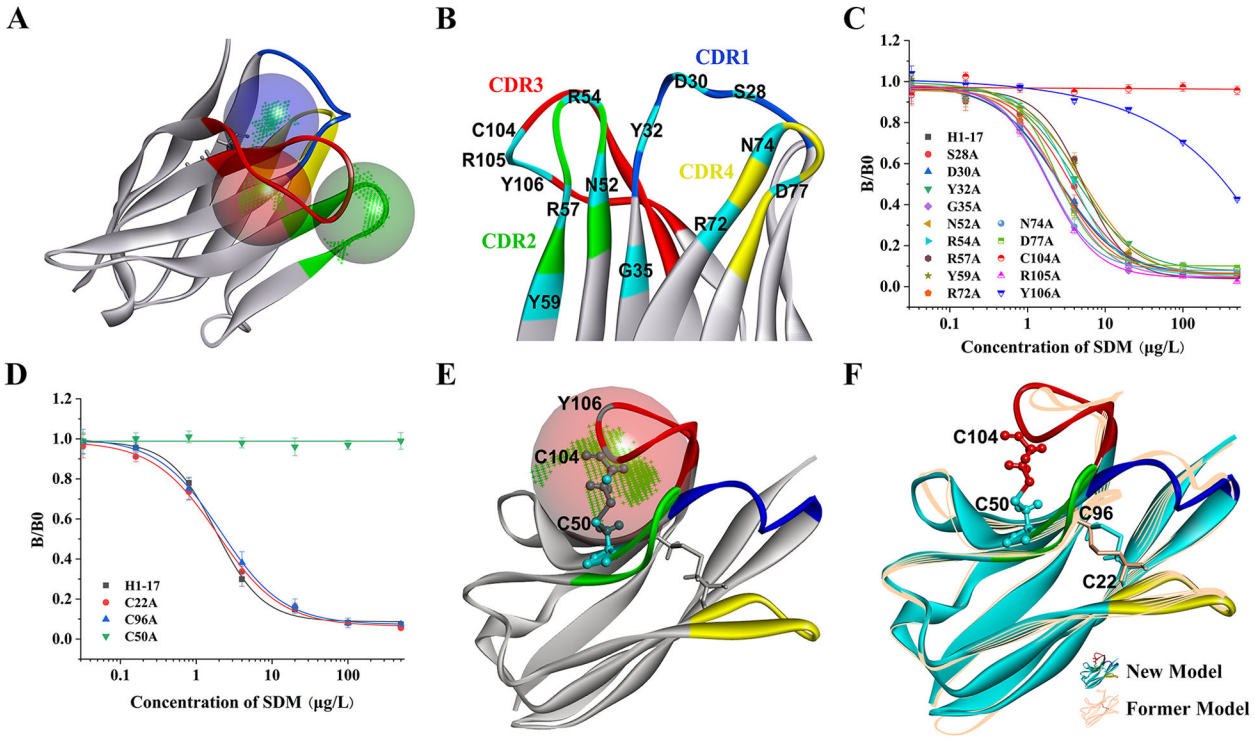

Fig. 5.

Molecular modeling and mutation of H1–17. (A) Possible binding sites of the first model. (B) Selected mutation sites based on the interaction between SDM and the first model. (C) The binding ability of H1–17 and its 14 mutants to SDM based on ic-ELISA inhibition curves. (D) The binding ability of the other three cysteine-mutations to SDM, including two conserved cysteines (C22 and C96) and the extra C50. (E) New model with two disulfide bonds and the confirmed binding site. (F) Structure alignment of two homology models. The noncanonical disulfide bond (C50-C104) in the new model is shown as ball and stick, and the conserved disulfide bond (C22-C96) in both models is shown as stick. CDR1–4 are colored blue, green, red, and yellow, respectively.

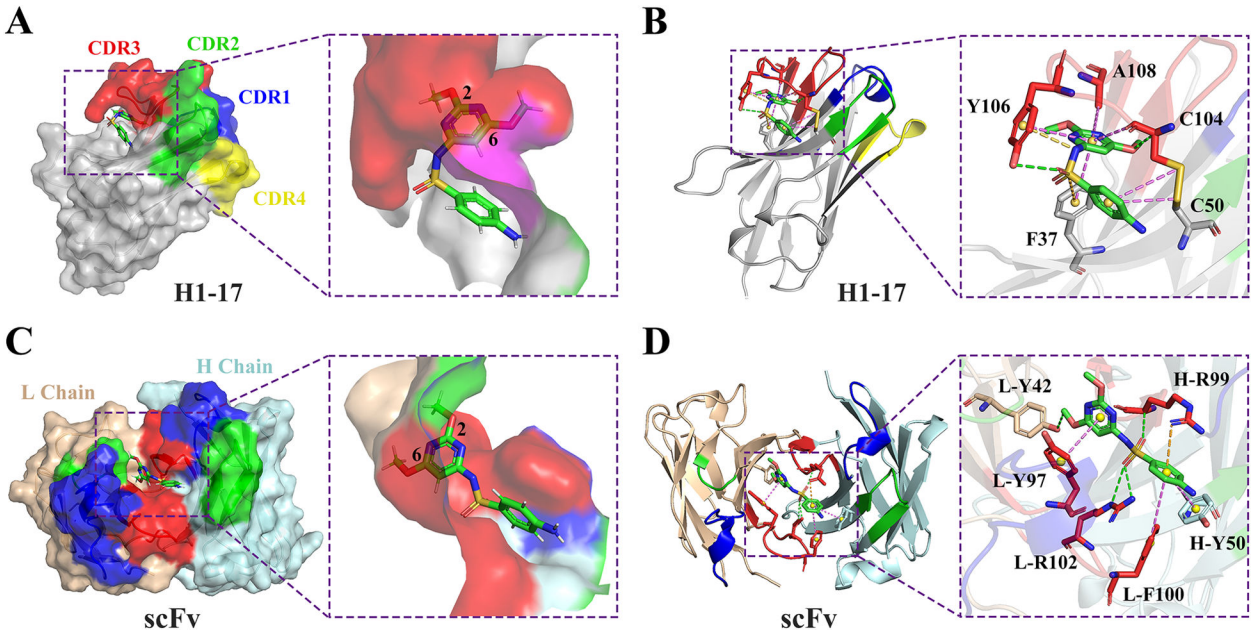

Fig. 6.

Molecular docking of H1–17 and scFv with SDM. (A) The overall structure of SDM binding to H1–17 and the orientation of SDM in the binding pocket. (B) The interaction between SDM and H1–17. (C) The overall structure of SDM binding to scFv and the orientation of SDM in the binding pocket. (D) The interaction between SDM and scFv. Hydrogen bonds, π-anion/π-cation, π-sulfur, and hydrophobic interactions are colored green, yellow, orange, and pink, respectively. CDR1–4 are colored blue, green, red, and yellow, respectively. C50 and C104 of H1–17 are colored magenta in the magnified binding pocket (right part of A).

Table 1.

The panning conditions and the corresponding output and enrichment results.

Round	SA10-X-OVA Concn. (μg/mL)	Other 28 SAs Concn. (μg/L)	SDM Elution Concn. (μg/L)	Input (cfu)	Output (cfu)	Enrichment
1	10	\	Gly-HCl	1×10^{12}	1.3×10^{7}	--
2	10	\	1000	1×10^{11}	2.3×10^{6}	--
3	10	20	1000	1×10^{11}	1.1×10^{4}	--
4	1	200	100	1×10^{11}	1.7×10^{5}	15.5
5	0.1	\	10	1×10^{11}	5.8×10^{6}	34.1

Note: \ means not used for panning; -- means no enrichment.

Table 2.

Kinetic parameters of H1–17 and other antibodies.

Antibodies	Analytes	k_a (1/Ms)	k_d (1/s)	K_D (M)
H1–17	SDM	1.29×10^{6}	1.36×10^{-3}	1.05×10^{-9}
H1–17	SA10-X-OVA	5.25×10^{4}	1.75×10^{-4}	3.33×10^{-9}
4C7	SDM	1.03×10^{4}	3.80×10^{-5}	3.69×10^{-9}
4D11	SDM	3.64×10^{4}	8.76×10^{-8}	2.41×10^{-12}

Table 3.

Binding modes of different nanobody-hapten complexes.

Target Names	Molecular Weights (Da)	Length of CDR1–4 (amino acids)	Number (location) of Cysteines	Number of Disulfide Bonds	Binding Modes	PDB Entry	Reference
Azo-dye RR6	733.38	11, 8, 18, 8	2 (FR1, FR3)	1	Conventional: CDR1 + CDR2 + CDR3	1QD0	Spinelli et al., 2000
Azo-dye RR1	612.56	8, 13, 17, 8	2 (FR1, FR3)	1	Conventional: CDR2 + CDR3	1I3U	Spinelli et al., 2001
MTX	454.44	8, 8, 17, 8	2 (FR1, FR3)	1	CDR1 tunnel + CDR4	3QXV/ (3QXT)	Fanning and Horn, 2011
TCC	315.58	8, 8, 17, 8	2 (FR1, FR3)	1	CDR1 tunnel + CDR4	5VL2	Tabares Da Rosa et al., 2019
Cortisol	362.46	8, 10, 17, 8	2 (FR1, FR3)	0	CDR1 tunnel + CDR4	6ITP/ (6ITQ)	Ding et al., 2019
SDM	310.33	8, 8, 14, 8	4 (FR1, FR2, FR3, CDR3)	2	CDR3 + Disulfide bond	\	This work

Table 4.

Mean recoveries (MR) and coefficients of variation (CV) of ic-ELISA for SDM in river water and whole milk samples with and without other SAs interference. (n = 3)

Spiked Levels (μg/L)		River water		Spiked Levels (μg/L)		Whole milk	
SDM	**Other SAs**	**MR (%)**	**CV (%)**	**SDM**	**Other SAs**	**MR (%)**	**CV (%)**
10	0	106.1	9.2	3	0	100.2	12.7
20	0	98.2	4.6	6	0	104.7	5.4
40	0	94.6	8.3	12	0	114.0	3.2
10	10	103.5	10.9	3	3	98.6	10.3
20	20	101.6	3.1	6	6	99.3	7.7
40	40	92.5	9.4	12	12	110.9	6.8